Protecting critical electronic equipment of UAVs against conducted UWB pulses

Alexey Vavilonsky
Television and Control Departamet Tomsk State University of Control Systems and Radioelectronics
Tomsk, Russian Federation
lexa060602@gmail.com

Dmitriy Petukhov
Television and Control Departamet Tomsk State University of Control Systems and Radioelectronics
Tomsk, Russian Federation
dimasuper06@bk.ru

Alexandr Kornev
Television and Control Departamet Tomsk State University of Control Systems and Radioelectronics
Tomsk, Russian Federation
kornev12333@mail.ru

Anton Belousov
Television and Control Departamet Tomsk State University of Control Systems and Radioelectronics
Tomsk, Russian Federation
anton.belousov@tu.tusur.ru

***Abstract*—For the first time, the paper considers the possibility of complex application of protective devices as part of unmanned aerial vehicles (UAVs) of rotorcraft and aircraft types to protect against ultra-wideband UWB pulses. The main radio-electronic equipment (REE) in the UAV and the ways of UWB pulse propagation along their circuits were determined. As protective devices, we selected a meander line with two separate turns, a strip modal filter (MF) with broad-side coupling, as well as MFs based on 4- and 6-conductor cable structures. We also analyzed and evaluated the effectiveness of the proposed approaches to ensuring electromagnetic compatibility of REE as part of UAVs under the excitation of conducted UWB pulse.**

Keywords—unmanned aerial vehicles, electromagnetic compatibility, modal filters, protective cables, meander lines.

I. INTRODUCTION

Currently, there is a tendency to use unmanned aerial vehicles (UAVs) in a wide variety of areas of human activity[1]. They find their application both in the civil (forestry and oil-and-gas industry, film industry, mapping, monitoring, etc.) and in the military areas. For example, armed forces of most developed countries use UAV resources for video and photography, monitoring, retransmission of radio signals, delivery, reconnaissance, guidance, damage during combat operations, etc. Because of wide capabilities of UAVs, many countries are developing and adopting not only their complexes, but also various means of countering them. The example is EMI-based functional destruction systems emitting high power UWB pulses. Meanwhile, their effectiveness directly depends on knowledge of the specific characteristics and elements of radio-electronic equipment (REE) as part of a specific UAV [2]. Such ultra-wideband (UWB) pulses of the nanosecond and subnanosecond ranges can penetrate into various nodes, blocks and circuits of REE disabling them. The result of such an excitation may be damage to integrated circuits and burnout of components, which leads to partial or complete failure of the REE.

There are several solutions to protect REE against UWB interference, including filters. At the same time, knowledge of the characteristics and features of real EMI-based functional destruction systems and, in particular, induced UWB interference, will allow you to make proactive and timely decisions, which can be a serious help during real combat operations [3]. Therefore, it is important to ensure electromagnetic compatibility (EMC) of REE as part of UAVs that can be located in the damage area of EMI-based functional destruction systems [3]. The task of providing EMC for specific REE as part of a UAV was first solved in 2022–2023 when the authors of the work carried out a project of the Russian Science Foundation. The aim of this work is to systematize the material obtained during the initial stages in to solving the tasks of this project. Thus, the paper provides a selection of specific UAVs and REE in their composition and justifies the choice. We provide details of their features and characteristics and evaluate the ways of of conducted UWB pulses propagation along REE circuits. We also analyze the possibility of increasing the protective characteristics of the selected REE when it is affected by EMI-based functional destruction systems.

The reported study was funded by the Russian Science Foundation, project number 24-29-00578.

II. SELECTION OF UNMANNED AERIAL VEHICLES AND THEIR RADIO-ELECTRONIC EQUIPMENT

Selection of UAVs was based on three main criteria: airframe size, payload, and available space (inside or outside the airframe) to install devices protecting against UWB pulses. Payload is a weight that does not affect the flight performance of the UAV, which it is able to lift without taking into account its own. In addition, an important criterion is the availability of information about materials and REE as part of the UAV in the public domain. Thus, a number of UAVs were considered, as well as their main characteristics required to solve the tasks set.

A. Rotorcraft unmanned aerial vehicles

Rotorcraft UAVs are conventionally divided into quadrocopters, hexacopters, and other multirotor platforms. Quadrocopters are rotary-wing UAVs with four rotors that provide vertical takeoff and landing, as well as allow maneuvering in the air. Hexacopters are equipped with six rotors, which provides additional stability and lift. In the following, we consider a number of rotorcraft UAVs. First, we considered the Geprc Mark5 DC HD model [4] (Fig. 1).

Fig. 1. Geprc Mark5 DC HD

The payload of this UAV is 230 g (the total weight, including the battery, is 600 g). An additional video camera, weighing 133–153 g, can also be installed on the upper part of the UAV, which covers most of the payload. The battery is located on the top of the UAV. Among other things, the free layout of the flight controller and the speed controller in the central part allows you to place interference protection devices by implementing a closer arrangement. Also, there is a sufficient amount of information in the public domain for a complete simulation of this UAV.

Then, the DJI Phantom 3 UAV was considered (Fig. 2) [5]. The weight of DJI Phantom 3 is 1216 g, and the maximum take-off weight declared by the manufacturer is 1500 g. Thus, the payload is 284 g. Nevertheless, the dense layout of the REE inside the UAV makes it impossible to install additional protection devices without violating the UAV design declared by the manufacturer. In addition, information about the REE in DJI Phantom 3 is not available for general use. For DJI series UAVs, the boards responsible for flight control are created to fit the dimensions of the airframe, so there is no data on the location of certain components on the board.

Fig. 2. DJI Phantom 3

In this work, attention is also paid to the rotorcraft UAV JMT F550 6-Aix (Fig. 3) [6]. In full assembly, the length, width, and height of the UAV are 600 mm, 530 mm, and 240 mm, respectively. The weight is 700 g, and the maximum take-off weight varies from 1400 to 1600 g (therefore, the payload is 700–900 g). At the same time, the UAV is equipped with a multi-tiered open-type housing, which allows installing additional protective devices. Table 1 summarizes the results of the selecting a rotorcraft UAV according to the criteria listed above.

Fig. 3. JMT F550 6-Aix

TABLE I. UAV CHARACTERISTICS ACCORDING TO: 1 – PAYLOAD, G; 2 – DIMENSIONS, MM; 3 – AVAILABILITY OF FREE SPACE

	1	2	3
Geprc Mark5	230	160×160×75	Yes
DJI Phantom 3	284	300×300×160	No
JMT F550 6-Aix	700–900	600×530×240	Yes

Taking into account the above data, the most preferred UAV for the purpose of this study is JMT F550 6-Aix. It uses a wide range of REE: a video transmitter, a camera servo, engine speed controllers, an optical air flow sensor, LED systems, etc. In addition, there are basic systems responsible for directly fulfilling the purpose of the UAV: a flight controller, a radio receiver, a GPS module, a voltage regulator, and a battery (Fig. 4). These systems are directly involved in powering, controlling, navigating, and controlling the operation of the UAV.

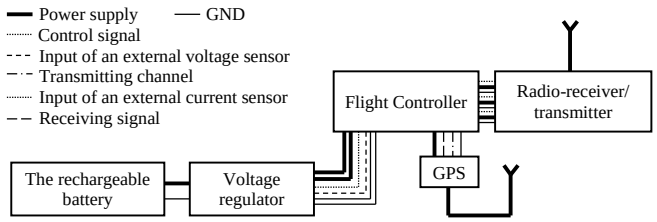

Fig. 4. Structural diagram of the JMT F550 6-Aix main systems with cable marking

Fig. 4 also shows the main cable connections of the REE. Knowledge of the parameters and types of cables used opens up the possibility of replacing them (while maintaining the characteristics of the useful signal) with protective structures designed to protect against UWB pulse.

As an example of a critical REE, we considered the GPS module. When it is exposed to a UWB pulse, the internal components of the REE can be degraded, and control over the UAV can be lost, which can result in the loss of the UAV. Let us consider the LEA-6H GPS module used in [7]. It is responsible for determining the location, orientation, and movement of the UAV in space. In addition, it ensures the accuracy and reliability of navigation data, which is necessary to perform a number of tasks, including surveillance, control, search, etc. [3]. The GPS module is equipped with a remote antenna (152 mm), and its operating voltage is 3.3 V.

As a result of the analysis of the GPS module used in the JMT F550 6-Aix, we propose several approaches to protect the modeule against UWB pulses. First, we propose a structural diagram of the REE as part of JMT F550 6-Aix that takes into account the use of MFs based on strip structures (Fig. 6). Then, for additional protection against UWB pulses, we propose to replace the available wires and cables with MFs based on cable structures by changing the location of individual wires and/or combining them into a single isolation. Finally, to prevent the possibility of crosstalk, as well as the impact of radiated UWB interference directly on the MF used, we propose to shield them by using enclosures (MFs based on strip structures) and materials such as shielding tapes/braids or foils (for MFs based on cable structures).

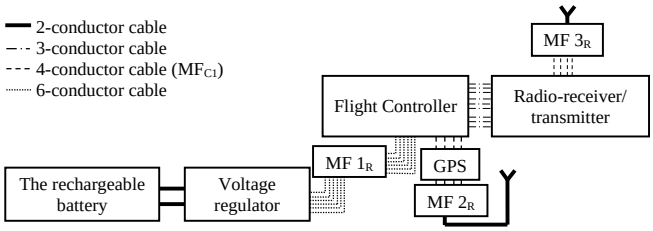

Fig. 5. Structural diagram of the JMT F550 6-Aix main systems taking into account protective devices

It can be seen from Fig. 6 that integration of MFs based on strip and cable structures is proposed between the critical elements of REE. Thus, MF 1 protects the flight controller from UWB pulses coming from the voltage regulator. MF 2_R and 3_R are installed next to antennas acting as the main receptor for induced interference. MF $1–3_R$ are made in the form of strip structures. It is also evident that 2-, 3-, 4- and 6-conductor MFs based on cable structures are used as part of the block diagram. As an example of a strip MF, in the next part of the work we will consider MF 2_R that is designed to protect the GPS module from conducted UWB pulse coming from the antenna. As an example of a cable structure, in the next part of the work we will consider 4-conductor MF_{C1} based on round cable.

B. Aircraft unmanned aerial vehicles

Next, aircraft-type UAVs were considered. They have various configurations, including models with a straight wing, gliders, aircraft with variable wing geometry, etc. Each of them has its own characteristics and advantages. Small UAVs with a straight wings are the most common type of aircraft UAVs. They provide flight range and efficiency, which allows them to perform various tasks, including surveillance, search and rescue operations, and scientific research. In the following, we consider a number of aircraft-type UAVs, as well as their main characteristics required to solve the tasks set. First, consider the ZOHD Drift UAV [8] (Fig. 6).

Fig. 6. ZOHD Drift

ZOHD Drift consists of EPP (foamed polypropylene) with a wingspan of 688 mm and a length of 877 mm. The assembled weight of the UAV is about 200 g, when the maximum take-off weight is 300 g. Thus, the payload is only 100 g. In addition, the presented UAV has a dense layout of REE in specialized compartments, which makes it difficult to place additional protective devices.

Then, the Sonicmodell AR Wing Pro UAV is considered (Fig. 7) [9]. This UAV is also made of EPP, the distance from the edge of the wing to the edge of the other wing is 1000 mm, and the length of the UAV is 450 mm. The weight of the UAV is 840 g, and the maximum take-off weight is 1425 g. Thus, the payload is 585 g. In the center of the case there is a compartment for installing a power supply and additional equipment, and at the back there is a compartment to locate the flight controller, ESC modules, and GPS module. Meanwhile, the dense internal REE layout allows the installation of a limited number of protective devices. The length, width, and height of the front compartment of the UAV are 156 mm, 138 mm, and 53 mm, respectively. The length, width, and height of the rear compartment are 90 mm, 110 mm, and 37 mm, respectively.

Fig. 7. Sonicmodell AR Wing Pro

Next, an aircraft–type UAV, the MFD Mini Crosswind 1600, is considered (Fig. 8) [10]. This UAV has a wingspan of 1600 mm, an airframe length of 1080 mm, and a maximum take-off weight of 5000 g. It is made of structural foam. The weight of this device without a battery is 1760 g. The payload of the UAV is more than 3000 g. The UAV airframe has a number of compartments suitable for installing additional equipment, which opens up the possibility of installing additional protective devices. Table 2 shows the results of selecting aircraft-type UAVs according to the criteria listed above.

Fig. 8. MFD Mini Crosswind 1600

TABLE II. UAV CHARACTERISTICS ACCORDING TO: 1 – PAYLOAD, G; 2 – DIMENSIONS, MM; 3 – AVAILABILITY OF FREE SPACE

	1	2	3
ZOHD Drift	100	688×877	Yes
Sonicmodell AR Wing Pro	585	1000×450	Yes
MFD Mini Crosswind 1600	3000	1600×1080	Yes

Taking into account the above data, the MFD Mini Crosswind is the most preferred UAV for the purpose of this study. The block diagram of REE as part of the Mini Crosswind 1600 is shown in Fig. 9. It can be seen that the selected UAV includes diverse REE, which are combined by means of cables. As part of this work, we will reflect the results of increasing the protective characteristics of one of the main UAV REE, the MFD Crosshair autopilot, when the equipment is exposed to conducted UWB pulse,.

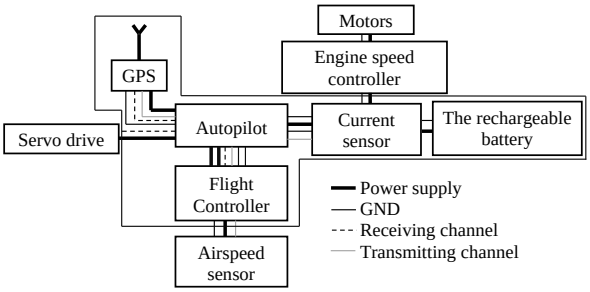

Fig. 9. Structural diagram of the MFD Mini Crosswind 1600 main systems with cable marking

The MFD Crosshair autopilot performs the functions of stabilizing the camera, ensuring mobility, eliminating potentially dangerous UAV movement parameters, etc. It is equipped with the following built-in sensors: gyroscope, accelerometer, electronic compass, and barometer. This model has two main processors for flight control and flight logic information processing. The device has an operating input voltage range of 7–26 V; and the manufacturer's recommended operating voltage is 12 V.

To protect the autopilot from the exciting UWB pulse, we propose to include a number of MFs based on strip and cable structures in the UAV, as shown in the block diagram of in Fig. 10. In addition, to prevent crosstalk between adjacent boards, as well as the impact of radiated UWB interference directly on the MFs used, the MFs are shielded with enclosures (for MFs based on strip structures) and materials such as shielding tapes/braids or foils (for MFs based on cable structures).

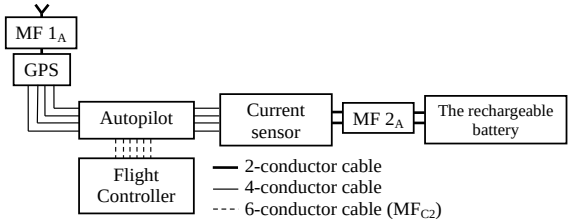

Fig. 10. Structural diagram of the MFD Mini Crosswind 1600 main systems taking into account protective cables

Fig. 10 shows that MF 1_A is installed between the GPS module and the antenna since the antenna in the UAV is the main receptor for UWB interference. MF 2_A is installed between the current sensor and the battery for additional protection of this segment of the electrical circuit from conducted UWB pulses. As an example of a strip MF, we will further consider the use of MF 2_A, and as a cable one – 6-conductor MF_{C2} based on round cable.

III. Methods and Approaches for Simulating

The MF 2_R was simulated in the TALGAT system [11] and took into account the losses. The MF 2_R in JMT F550 6-Aix is a meander microstrip line (MSL) with two separate turns. The cross section of MF 2_R in the shielding enclosure is shown in Fig. 11*a*, where w is the width of the conductors, s_i is the gap between the conductors, t is the thickness of the conductors, h is the thickness of the substrate, d is the distance from the edge of MF to the nearest MF conductors, and ε_{ri} is the relative permittivity of the substrate. Optimization was performed by heuristic search by amplitude and time criteria to reduce the level of UWB pulse at the MF output. The MF equivalent circuit is shown in Fig.f 12*a*. The length (l) of MF was 1.2 m (MF 2_R), and the values of the resistances R_G, R_L and R were 50 Ω each. The parameters of the exciting UWB pulse were as follows: the amplitude of the EMF of 500 V, the duration of the front, fall, and flat top of 42 ps, 30 ps and 4 ps (at levels of 0.1–0.9), so that the total duration (at level 0.5) was 60 ps [12].

The MF 2_A in the Mini Crosswind 1600 is a strip structure with a broad-side coupling. Its cross-section (with optimal parameters) in the shielding enclosure is shown in Fig. 11*b*. The MF equivalent circuit is shown in Fig. 12*b*. The MF length was l=1 m (MF 2_A), and the values of R_G, R_L and R were 50 Ω each. The parameters of the UWB pulse remained unchanged.

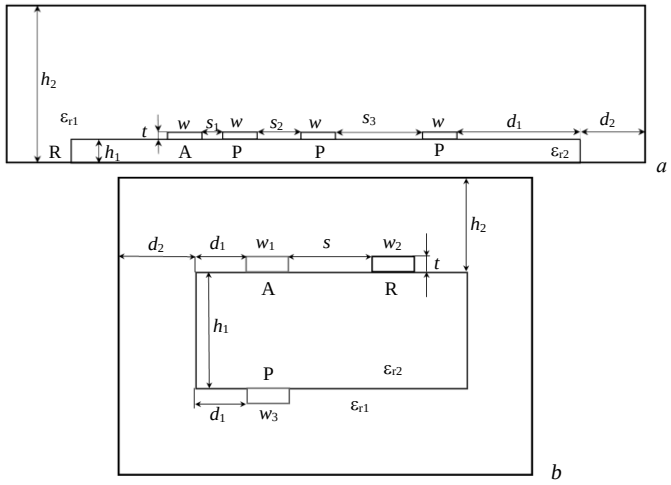

Fig. 11. Cross section of the meander line with two separate turns (*a*) and MF with a broad-side coupling (*b*)

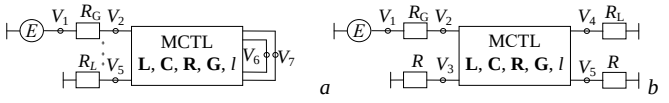

Fig. 12. Equivalent circuit of the meander line with two separate turns (*a*) and MF with a broad-side coupling (*b*)

As noted earlier, we proposed to replace a number of cable/wire connections between UAV REE with MF_{C1} while maintaining their performance characteristics. Thus, in the factory assembly of JMT F550 6-Aix, 4 separate single-core wires are laid between the flight controller and the GPS module. Consider the option when these wires are combined into one 4-conductor shielded cable MF_{C1}. The cross section of such MF_{C1} is shown in Fig. 13*a*, where $r_{1\text{-}2}$ is the radius of the conductors, $r_{3\text{–}4}$ is the radius of insulation around the conductors, r_5 is the radius of internal insulation, and r_6 is the radius of external insulation [13]. An equivalent circuit for the inclusion of this MF_{C1} is shown in Fig. 14*a*. The length of MF_{C1} is l=250 mm, and the values of R_G, R_L and R are 50 Ω each. The choice of length was determined by the length of the

source wires. The parameters of the UWB pulse remained unchanged.

6 single-core wires are laid between the flight controller and the autopilot in the Mini Crosswind 1600. To add additional protection, we proposed to replace them with MF_{C2} based on a cable structure (while maintaining the same operating mode) to add additional protection to the UAV REE system. The cross section of such an MF_{C2} is shown in Fig. 13*b*, where $r_{1\text{-}5}$ is the radius of the conductors, r_6 is the radius of insulation around the conductors, r_7 is the radius of internal insulation, and r_8 is the radius of external insulation. An equivalent circuit for the inclusion of this MF_{C2} is shown in Fig. 14*b*. The length of MF_{C2} is l=400 mm, and the values of R_G, R_L and R are 50 Ω each. The parameters of the UWB pulse remained unchanged.

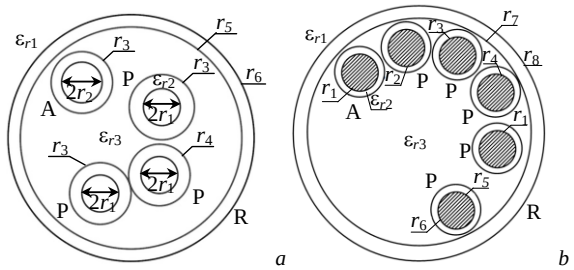

Fig. 13. Cross section of the 4- (*a*) and 6-conductor (*b*) MF_{C1} and MF_{C2} based on a cable structure

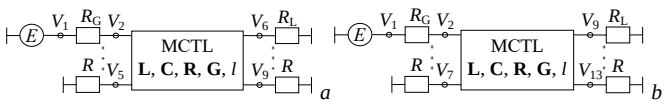

Fig. 14. Equivalent circuit of the 4- (*a*) and 6-conductor (*b*) MF_{C1} and MF_{C2} based on a cable structure

IV. Simulation Results

This section presents the results of simulating the proposed MF configurations. Thus, we optimized the geometric parameters of MF 2_R as part of the JMT F550 6-Aix UAV. The resulting parameters are the following: w=300 μm, s_1=220 μm, s_2=450 μm, s_3=640 μm, t=35 microns, d_1=900 μm, d_2=1500 μm, h_1=200 μm, h_2=1635 μm, l=1200 mm, and ε_{r1}=1. The resulting parameters of the MF 2_A as part of the Mini Crosswind 1600 UAV are the following: w=400 μm, s=400 μm, t=35 μm, d_1=400 μm, d_2=1200 μm, h_1=1000 μm, h_2=1200 μm, l=1000 mm, and ε_{r1}=1. As the substrate, we chose the Arlon AD 1000 composite material with a relative permittivity value ε_{r2}=10 and a tangent of the dielectric loss angle tgδ=0.025.

Similarly, we optimized the geometric parameters of the 4-conductor MF 1 based on cable structures. The resulting parameters of this MF_{C1} as part of the JMT F550 6-Aix UAV are the following: r_1=0.3 mm, r_2=3 mm, r_3=0.5 mm, r_4=0.53 mm, r_5=2 mm, r_6=1.8 mm, ε_{r1}=1, ε_{r2}=7, and ε_{r3}=4.2. The results of optimization of the 6-conductor MF_{C2} as part of the Mini Crosswind 1600 UAV are as follows: r_1=0.15 mm, r_2=0.12 mm, r_3=0.13 mm, r_4=0.14 mm, r_5=0.16 mm, r_6=0.25 mm, ε_{r1}=1, ε_{r2}=7 and ε_{r3}=4.2.

A. Modal filters based on strip structures

Fig. 15 shows the waveforms of EMF, input and output voltages of the MF 2_R included between the GPS module and the antenna in the JMT F550 6-Aix UAV. Fig. 16 shows the waveforms of EMF, input and output voltages of the MF 2_A, connected between the current sensor and the battery in the Mini Crosswind 1600 UAV.

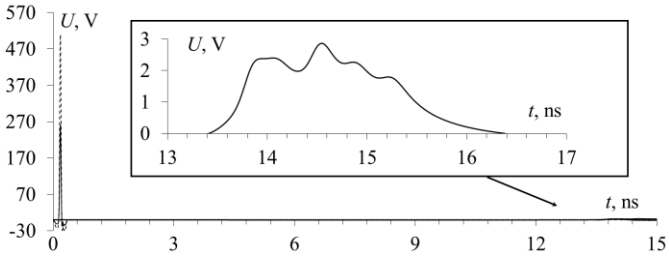

Fig. 15. Waveforms of EMF (- -), input (–) and output (–) voltages of MF 2

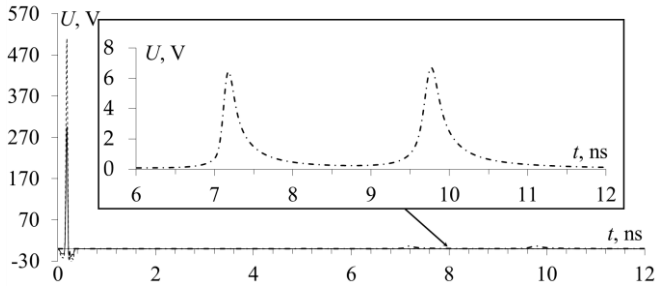

Fig. 16. Waveforms of EMF (-·-), input (–) and output (- -) voltages of MF 2

It can be seen from Fig. 15 that the exciting UWB pulse (250 V) was reduced to 2.86 V. Thus, the maximum output voltage of MF 2_R does not exceed the maximum input voltage of the GPS module (3.3 V). A sequence of partially superimposed decomposition pulses is observed at the MF output. This can be explained by the fact that the difference in delays of the nearest decomposition pulses is less than the duration of the exciting pulse. This can also be caused by dispersion and losses in the transmission line. As a result of using MF 2_R, it was possible to obtain an 87-fold attenuation of the UWB pulse. To integrate MFs into the UAV airframe, it is necessary to trace them taking into account the free space in the UAV airframe. With this in mind, the MF conductors was «rolled up» into turns with a weak electromagnetic coupling between them (3*w*) [13]. This allowed obtaining the final dimensions of the MF 2_R printed circuit board of 78.5×80 mm^2.

Fig. 16 shows that 2 main pulses with a maximum amplitude of 6.6 V arrive at the MF 2_A output, so the maximum output voltage does not exceed the maximum (26 V) and the manufacturer's recommended (12 V) input voltage of the autopilot board. Hence, the attenuation coefficient of MF is 42 times (relative to the input voltage of 280 V). Tracing this MF allowed us to obtain the final dimensions of the MF 2_A printed circuit board of 59×60 mm.

B. *Modal filters based on cable structures*

The waveforms of EMF, input and output voltages of 4- and 6-conductor MFs are shown in Figs. 17 and 18.

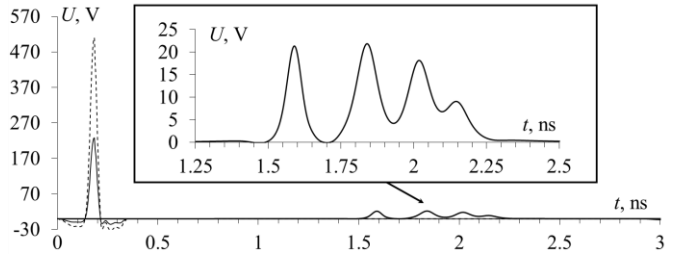

Fig. 17. Waveforms of EMF (- -), input (–) and output (–) voltages of a 4-conductor MF based on a cable structure

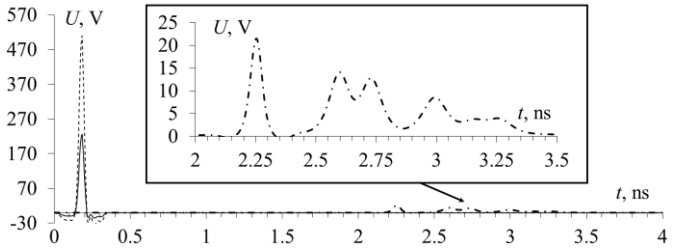

Fig. 18. Waveforms of EMF (- -), input (–) and output (-·-) voltages of a 6-conductor MF based on a cable structure

Fig. 17 shows that 4 main pulses with a maximum amplitude of 21.87 V arrive at the output of MF_{C1}. At the same time, the maximum operating voltage of the flight controller is 22 V. In this case, between 1 and 2, as well as 2 and 3 pulses, a condition is provided in which the difference in delays of the decomposition pulses is greater than the duration of the exciting pulse. Their partial overlap, in turn, is explained by the effect of losses and dispersion in the cable structure. As a result, it was possible to weaken the excitation UWB pulse by 11.9 times (compared to the input voltage of 250 V).

Fig. 18 shows that 6 main pulses with a maximum amplitude of 21.5 V come to the output of MF_{C2}. At the same time, the maximum operating voltage of the flight controller is 22 V. In this case, between 1, 2, 3, 4 and 5 and 6 pulses, a condition is provided in which the difference in delays of the decomposition pulses is greater than the duration of the exciting pulse. Their partial overlap is explained by the effect of losses and dispersion in the cable structure. As a result, the excitation UWB pulse was attenuated by 10.2 times (compared with the input voltage of 220 V).

V. Conclusion

To provide EMC in terms of protecting REE as part of the UAV from the UWB pulses, 2 different MFs were used as structures with modal techniques: based on a meander MSL with two separate turns and based on a 4-conductor round cable. MFs based on a meander MSL with two separate turns, switched on between the GPS module and the UAV antenna, attenuated the UWB pulse (250 V) to 2.86 V at the maximum operating voltage of the GPS module LEA-6H of 3.3 V. The attenuation coefficient of the UWB pulse was 87 times. MFs based on a 4-conductor round cable allowed the UWB pulse to be decomposed into 4 modes with a maximum voltage of 21.87 V (with the attenuation coefficient of 11.9 times).

The MFD Mini Crosswind 1600 UAV was considered in the work. A block diagram of the main REE in this UAV was designed and modified, and the propagation of conducted UWB pulses was assessed. As protective devices against the excitation of UWB pulses, we considered an MF based on a strip structure with a broad-side coupling and a 6-conductor MF based on a round cable structure. The effectiveness of the proposed approaches to providing EMC was evaluated in terms of protecting UAV REE from the effects of conducted UWB pulses. The results of this work may be useful to UAV developers, as they open up the possibility of developing REE for UAV with an increased level of UWB pulse protection.

References

[1] S.I. Makarenko, Countering unmanned aerial vehicles, systems of control, communication and security, St.Peterburg, science-intensive technologies, 204 p., 2020.

[2] Arsenal-otechestva, “Methods of countering UAVs,” [Online]. Available: https://arsenal-otechestva.ru/article/1601-metody-protivodejstviya-bpla [Accessed: September 14, 2023].

[3] A.O. Belousov, “Approaches to ensuring electromagnetic compatibility of radioelectronic devices as part of a complex of functional destruction of unmanned aerial vehicles by powerful electromagnetic radiation,” no. 3, pp. 134-196, 2023, DOI: 10.24412/2410-9916-2023-3-134-196.

[4] Dronomania, “Geprc Mark 5 DC HD: for freestyle and FPV shooting,” [Online]. Available: Geprc Mark 5 DC HD: for freestyle and FPV shooting [Accessed: March 26, 2023].

[5] DJI Phantom 3, “DJI Phantom 3 overview, specifications, instructions,” [Online]. Available: https://dronnews.ru/obzory/dji/dji-phantom-3-standard.html [Accessed: March 27, 2023].

[6] Stelashop, “JMT F550 6-Aix: overview, characteristics,” [Online]. Available: https://strelashop.ru/product/32810864322 [Accessed: February 12, 2024].

[7] Lyvi, “Gps with compass,” [Online]. Available: https://lyvi.ru/p-4000016400431 [Accessed: February 12, 2024].

[8] Aliexpress, “ZOHD Drift,” [Online]. Available: https://aliexpress.ru/item/1005003285033178.html?sku_id=12000033272463804 [Accessed: February 12, 2024].

[9] Fpvwingrc, “Sonicmodell Ar Wing Pro,” [Online]. Available: https://fpvwingrc.ru/product/sonicmodell-ar-wing-pro-radioupravlyaemyj-samolet-1000-mm-razmah-krylev-epp-fpv-letajushhaya-model-kryla-polnostju-sobrano-i-gotova-k-poljotu/ [Accessed: February 12, 2024].

[10] Banggood, “MFD Mini Crosswind 1600,” [Online]. Available: https://ru.banggood.com/New-MyFlyDream-MFD-Mini-Crosswind-1600mm-Wingspan-EPO-Aerial-Survey-Aircraft-FPV-Platform-Mapping-UAV-RC-Airplane-KIT-p-1546242.html [Accessed: February 12, 2024].

[11] Talgat, “TALGAT system is a software package for modeling electromagnetic compatibility problems,” [Online]. Available: https://talgat.org/talgat-software/ [Accessed: February 12, 2024].

[12] A. O. Belousov, “Analysis and optimization of multi-conductor structures with modal decomposition for processing pulse signals. Dissertation of the Candidate of Technical Sciences: 05.12.04, p. 247, 2020.

[13] A.O. Belousov, N.O. Vlasova, V.O. Gordeyeva, T.R. Gazizov, “Breaking the Symmetry of Cable Structures as an Instrument for Improving Modal Decomposition to Protect Critical Equipment Against UWB Pulses,” vol. 14(6), no. 1228, pp. 1–34, 2022.